

Asian Power Electronics Journal

PERC, HK PolyU

Copyright © The Hong Kong Polytechnic University 2021. All right reserved.

No part of this publication may be reproduced or transmitted in any form or by any means, electronic or mechanical, including photocopying recording or any information storage or retrieval system, without permission in writing form the publisher.

First edition December 2021 Printed in Hong Kong by Reprographic Unit.
The Hong Kong Polytechnic University

Published by

Power Electronics Research Centre
The Hong Kong Polytechnic University
Hung Hom, Kowloon, Hong Kong

ISSN 1995-1051

Disclaimer

Any opinions, findings, conclusions, or recommendations expressed in this material/event do not reflect the views of The Hong Kong Polytechnic University

Editorial board

Honorary Editor

Prof. Fred C. Lee, Electrical and Computer Engineer, Virginia Polytechnic Institute and State University

Editor

Victor Electronic Ltd.

Associate Editors and Advisors

Prof. Philip T. Krien
Department of Electrical and Computer Engineering, University of Illinois

Prof. Keyue Smedley
Department of Electrical and Computer Engineering, University of California

Prof. Muhammad H. Rashid
Department of Electrical and Computer Engineering, University of West Florida

Prof. Dehong Xu
College of Electrical Engineering, Zhejiang University

Prof. Hirofumi Akagi
Department of Electrical Engineering, Tokyo Institute of Technology

Prof. Xiao-zhong Liao
Department of Automatic Control, Beijing Institute of Technology

Prof. Hao Chen
Department of Automation, China University of Mining and Technology

Prof. Danny Sutanto
Integral Energy Power Quality and Reliability Centre, University of Wollongong

Prof. S.L. Ho
Department of Electrical Engineering, The Hong Kong Polytechnic University

Prof. Eric K.W. Cheng
Department of Electrical Engineering, The Hong Kong Polytechnic University

Dr. Norbert C. Cheung
Department of Electrical Engineering, The Hong Kong Polytechnic University

Dr. Edward W.C. Lo
Department of Electrical Engineering, The Hong Kong Polytechnic University

Dr. Martin H. L. Chow
Department of Electrical Engineering, The Hong Kong Polytechnic University

Dr. Chi Kwan Lee
Department of Electrical and Electronic Engineering, The University of Hong Kong

Publishing Director:

Prof. Eric K.W. Cheng, Department of Electrical Engineering, The Hong Kong Polytechnic University

Communications and Development Director:

Dr. James H.F. Ho, Department of Electrical Engineering, The Hong Kong Polytechnic University

Production Coordinator

Dr. Jinghong Sun, Dr. Xiaolin Wang, and Dr. Zilin Li, Power Electronics Research Centre, The Hong Kong Polytechnic University

Secretary:

Ms. Kit Chan, Department of Electrical Engineering, The Hong Kong Polytechnic University

Table of Content

Design and Evaluation of a Phase-Shift Full-Bridge Converter for Electrical Vehicle	1
Shisong Wang, Yuanxiong Duan, Jinhao Ruan, Zhanghai Shi	
Energy Storage, Fuel Cell, and Electric Vehicle Technology	6
Cheng K.W.E.	
Study and Development of Mixed Repurposing EV Battery System for Stationary Energy Storage Applications	11
Y.C. Fong, D. H. Wang, J. Mei, S. Raghu Raman, and K.W.E. Cheng	
Author Index	17

Design and evaluation of a phase-shift full-bridge converter for electrical vehicle

Shisong Wang, Yuanxiong Duan, Jinhao Ruan, Zhanghai Shi

Department of Electrical Engineering, Southwest Jiaotong University, Chengdu, China

E-mail: shizhanghai@163.com

Abstract –A high frequency converter with maximum 150A/2.5kW output is designed and evaluated in this paper. This converter consists of three parallel PSFB modules. The main components for each module are designed. Small signal model for single module is established and a digital peak current mode control is designed and implemented. Finally, a 2.5kW prototype with up to 150A output current is built. The experimental results demonstrate well performance of the prototype and confirm of the validity the design.

Keywords – phase-shift full-bridge; small signal model; peak current mode control

I. INTRODUCTION

There are many low-voltage electronic devices on electric vehicles, such as air conditioner, wiper, multimedia equipment and lighting system. These electronic devices work with low voltage, but the total current of these loads is high. Therefore, a low-voltage and high-current power supply is required, which converts the high voltage of vehicle power battery to low voltage and provides high current.

Phase-shift full-bridge (PSFB) DC-DC converter have the advantages such as high-power density, low switching loss and large conversion ratio, thus it is widely applied in high-power and high-frequency isolated power conversion system.

Series studies on PSFB converter have been carried out [1]-[7]. PSFB ZVS DC-DC converter can realize zero voltage switching (ZVS), thus switching loss can be significantly reduced, but the ZVS range of switches (especially in lag bridge) is limited and may loss ZVS at light load. Many approaches of keeping ZVS of PSFB converter at light load have been reported, for example, an auxiliary circuit attached to the main circuit is designed to achieve ZVS at light load in [3], and [4]-[6] report some control strategies to extent ZVS range. The loss of diode rectifier will be significant under large output current, to increase the efficiency, synchronous rectifier is applied in [7-8] to reduce power loss of rectification circuit, and the power loss of synchronous rectifier is analyzed in [8].

Peak current mode control (PCMC) is widely used in control of DC power supply attributed to the advantages such as inherent over current protection, automatic current sharing in parallel operation. In [9] and [10], PCMC is applied to control the isolated DC-DC converter, and the digital slop compensation of PCMC is studied in [11].

In this paper, a high-current power converter which consists of three PSFB modules is designed and evaluated. To

reduce loss, rectifier diodes are replaced by MOSFETs to achieve synchronous rectifier. A resonant inductor is applied to extend the soft switching range. Each module has a double-current-loop controller to regulate the output current. PCMC is used as the inner-loop controller which can prevent the transformer saturation.

The rest of this paper is organized as follows. In section II, the circuit topology and parameter design are introduced; to design the controller, the small signal model is established in section III; and the experimental results of a 2.5kW prototype are presented in section IV. Finally, in section V, some conclusions are presented.

II. DESIGN OF MAIN CIRCUIT

A. Circuit topology

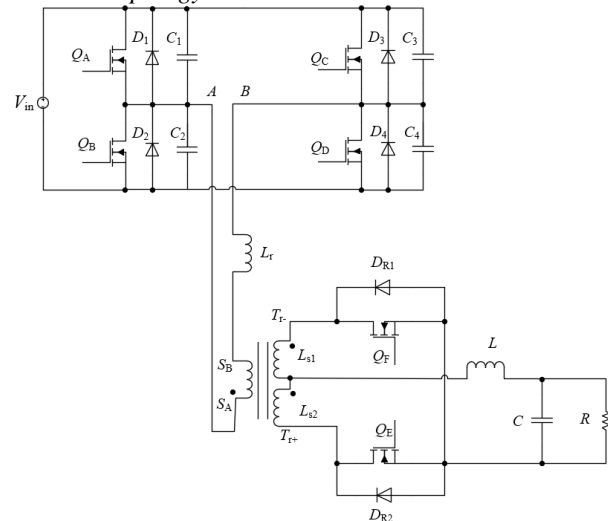


Fig. 1: The topology of synchronous rectified PSFB circuit

Fig.1 is the topology of single PSFB converter with synchronous rectifier. The primary side is a full-bridge inverter consists of MOSFET $Q_1 \sim Q_4$, and the secondary side is a synchronous rectifier circuit, using MOSFET with lower on-resistance to replace diodes, thus the loss of rectifier can be effectively reduced, and the efficiency of converter can be increased. In Fig. 1, $C_1 \sim C_4$ are the parasitic capacitance of MOSFET. Usually, their capacitance is not large enough to implement soft switching. It is necessary to add extra capacitor to them. L_r is the resonant inductor, its value equals to the sum of circuit parasitic inductance and transformer equivalent leakage inductance. The PSFB converter can achieve ZVS through the resonance of L_r and $C_1 \sim C_4$. The turns ratio of transformer is $n: 1: 1$ which is determined by requirement of input and output voltage range. The circuit of output filter consists of inductor L and capacitor C . And R is the load.

Fig. 2 shows the operation waveforms of PSFB converter with synchronous rectifier. The output voltage of PSFB converter can be adjusted by the phase difference between two bridge legs. And the detailed operation principle can be found in [8].

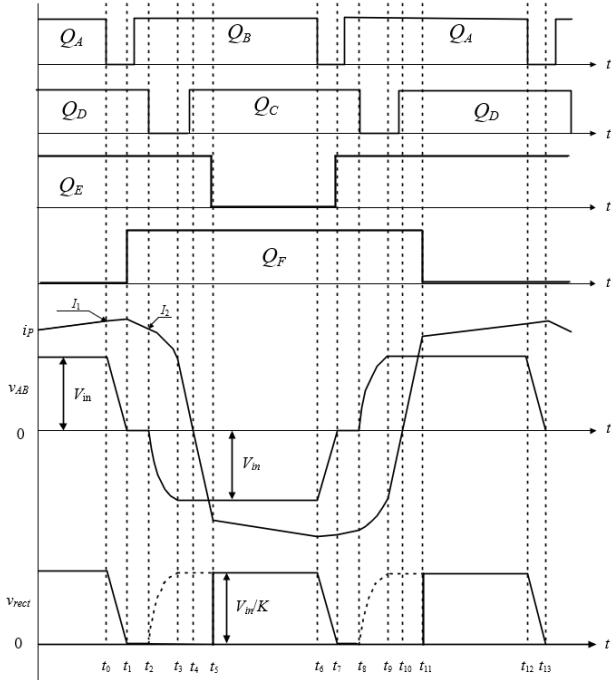


Fig. 2: The main waveforms of PSFB converter with synchronous rectifier

Parallel operation of PSFB modules can increase the output power or current. In the design of this paper, three parallel modules work together as Fig. 3.

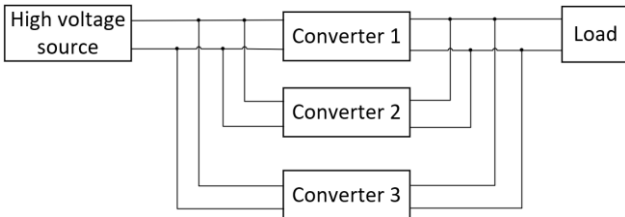


Fig. 3: The structure of three parallel PSFB

B. Design of circuit

The required specifications of the designed PSFB converter include input voltage DC 315-420V, controllable output current ranged from 0A to 150A, the 5A maximum current ripple, and the maximum output voltage 20V. As the converter is composed by three parallel PSFB modules, each module will take a load of 50A.

In PSFB converter, the switches of bridge can achieve ZVS by the resonance between leakage inductor of transformer and parasitic capacitor of switches[1]. An extra resonant inductor can help to keep the ZVS property at light load.

As Fig. 2 shows, the duty cycle of secondary voltage V_{rect} is smaller than primary voltage V_{AB} . The duty cycle loss of secondary voltage has been derived in [1]. It is expressed as (1).

$$D_{eff} = D - \frac{2kL_r f_s}{V_{in}} (2I_L - \frac{V_o}{2f_s L} (1-D)) \quad (1)$$

where $k = 1/n$ is the turns ratio between the secondary side and primary side of transformer, f_s is switching frequency, V_{in} and V_o are input voltage and output voltage, L_r is the value of resonant inductor and L is the value of output inductor, D is the duty cycle of primary side voltage V_{AB} .

From (1), a larger resonant inductance L_r means larger duty cycle loss D_{loss} , thus the resonant inductor should be set to an appropriate value. In this design, the resonant inductor is set to $L_r = 16 \mu H$. After some calculations, the parameters of the PSFB in Fig. 1 are designed as Table 1.

Table 1: Main circuit parameters

Items	Symbol	Value
Input voltage	V_{in}	DC 315V
Transformer ratio	$n: 1$	10:1:1
Maximum output voltage	V_o	DC 20V
Output current	I_o	50 A
Output filter inductor	L	300 μH
Resonant inductance	L_r	16 μH
Switching frequency	f_s	100 kHz
Output filter capacitor	C	5000 μF

III. SMALL SIGNAL MODELING AND CONTROLLER DESIGN

As Fig. 4 shows, a double-current-loop control system is designed to regulate the output current of converter, where inner loop is peak current mode controller. To design the controller of outer loop, small signal model of designed PSFB converter is established in this section.

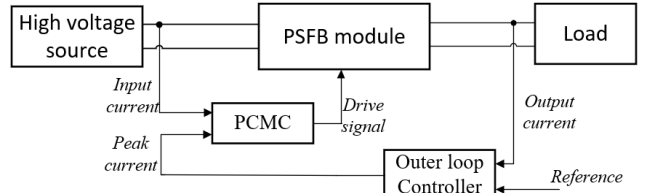


Fig. 4: The structure of proposed control system

A. Modeling of designed PSFB converter

PSFB converter is derived from Buck converter. It is a kind of isolated Buck converter, thus the small signal model of PSFB converter can refer to the model of Buck converter. But the loss of duty cycle and turns ratio of transformer should be considered. According to [1], the effective duty cycle perturbation can be derived as (2).

$$\hat{d}_{eff} = \hat{d} + \hat{d}_v + \hat{d}_i \quad (2)$$

where \hat{d}_i and \hat{d}_v are the perturbations of effective duty cycle resulting from the change of output filter current i_L and the change of input voltage V_g , respectively. And \hat{d} is the perturbation of duty cycle.

The established small signal model of designed PSFB DC-DC converter is shown in Fig. 5. From Fig. 5, the transfer

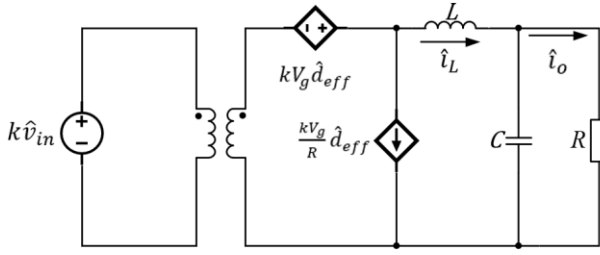
function from duty cycle \hat{d} to output current \hat{i}_o can be derived as (3).

$$G_{od}(s) = \left. \frac{\hat{i}_o(s)}{\hat{d}(s)} \right|_{\hat{v}_{in}=0} = \frac{kV_{in}}{RLCs^2 + (RR_d C + L)s + (R + R_d)} \quad (3)$$

where $R_d = 4k^2 f_s L_r$.

The transfer function from duty cycle \hat{d} to output filter inductor current \hat{i}_L is (4).

$$G_{id}(s) = \left. \frac{\hat{i}_L(s)}{\hat{d}(s)} \right|_{\hat{v}_{in}=0} = \frac{kV_{in}(RCs + 1)}{RLCs^2 + (RR_d C + L)s + (R + R_d)} \quad (4)$$



1: D_{eff}

Fig. 5: Small signal model of designed PSFB DC-DC converter

B. Modeling of controller

In this design, input current i_g is the input of inner-loop, and the feedback factor of current sensor is R_s . The waveform of PCMC in this PSFB converter is shown in Fig. 6, where m_c is the slope compensation of peak current i_c which helps to prevent sub-harmonic of PCMC, m_1 and m_2 are slopes of converted output inductor current i_L , and the period of i_g and i_L is $T = T_s/2$.

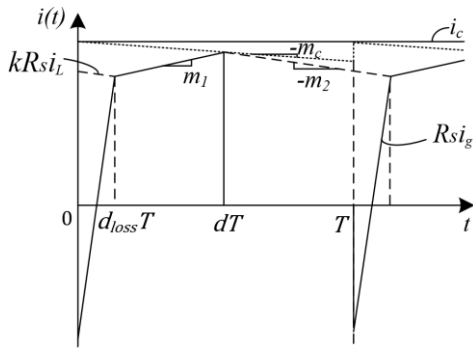


Fig. 6: Waveform of PCMC in PSFB converter

According to the operating principle of PSFB converter, i_g is equal to the converted output inductor current i_L during $d_{loss}T$ as Fig. 6 shows, thus the average value of $kR_s i_L$ in a period can be expressed as:

$$kR_s \langle i_L \rangle_T = \langle i_c \rangle_T - m_c dT - \frac{1}{2} m_1 d_{eff}^2 T - \frac{1}{2} m_2 (1 - d_{eff})^2 T \quad (5)$$

where

$$\begin{cases} m_1 = \frac{kR_s [kV_g - Ri_o]}{L} \\ m_2 = \frac{kR_s Ri_o}{L} \end{cases}$$

Removing the higher-order perturbations, the \hat{d} can be expressed as:

$$\hat{d} = F_d(\hat{i}_c - F_L \hat{i}_L - F_v \hat{v}_{in} - F_o \hat{i}_o) \quad (6)$$

where $F_d = \frac{1}{M_c T}$, $F_L = kR_s$, $F_v = \frac{k^2 R_s D_{eff}^2 T}{2L}$, $F_o = \frac{kR_s R(1 - 2D_{eff})T}{2L}$.

C. Modeling of closed-loop system

From equation (3) (4) and (6), the transfer function from control current \hat{i}_c to output current can be expressed as:

$$G_{oc}(s) = \left. \frac{\hat{i}_o(s)}{\hat{i}_c(s)} \right|_{\hat{v}_{in}=0} = \frac{F_d M_{od}(s)}{1 + F_d F_o M_{od}(s) + F_d F_L M_{id}(s)} \quad (7)$$

Thus, the block diagram of small-signal closed-loop system can be established as Fig. 7, where H_o is the feedback proportional coefficient of output current \hat{i}_o , and G_c is compensation function of outer-current-loop.

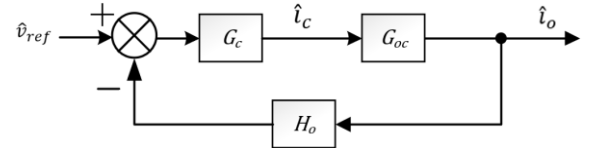


Fig. 7: The block diagram of small-signal closed-loop system

From Fig. 7, the open-loop transfer function can be deduced:

$$T_c = G_{oc} \cdot H_o \quad (8)$$

D. Controller design

The circuit parameters of this converter are set as Table. I, the resistance of load set to $R = 0.4 \Omega$, and $R_s = 51$, $H_o = 9.4$, the compensation slope of PCMC is set to $m_c = 3.1 \times 10^6$, from equation (8), the open-loop transfer function T_c can be calculated as:

$$T_c(s) = \frac{3.03 \times 10^7}{s^2 + 3.52 \times 10^4 s + 1.8 \times 10^5} \quad (9)$$

The bode diagram of T_c is shown in Fig. 8. A simple PI controller $G_c(s)$ is designed based on the T_c as equation (10).

$$G_c(s) = 0.1 + 200 \times \frac{1}{s} \quad (10)$$

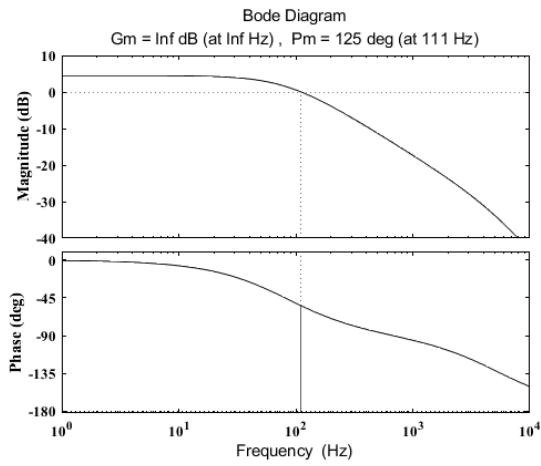


Fig. 8: The frequency response diagram of open-loop transfer function T_c

IV. EXPERIMENTAL RESULTS

Finally, a prototype of 2.5kW DC-DC converter consists of three parallel PSFB modules is given in Fig. 9, and the thermal imagery is given in Fig. 10. It can be noticed that each module takes 50A output current, and the overall temperature of converter is lower than 70 °C which is within the accepted range. Fig. 11 is the waveform of drain-source voltage of Q_B (channel 1), drain-source voltage of Q_D (channel 2), primary side voltage V_{AB} (channel 3) and primary side current i_p (channel 4) while input voltage is 100V. It can be noticed that the waveform is stable and ZVS has been achieved.

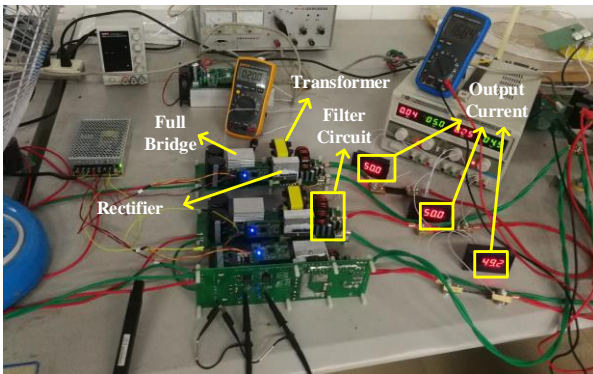


Fig. 9: Prototype of the three parallel PSFB converter



Fig. 10: Thermal imagery of the converter

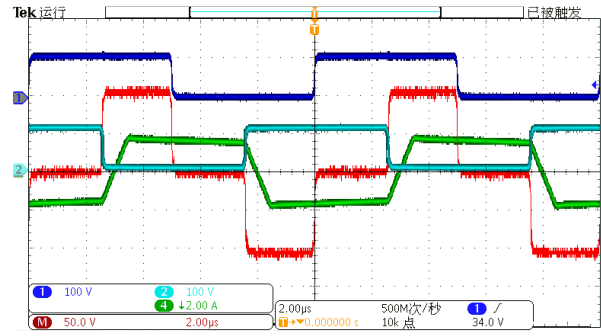


Fig. 11: The waveform of drain-source voltage of Q_B (channel 1), drain-source voltage of Q_D (channel 2), primary side voltage V_{AB} (channel 3) and primary side current i_p (channel 4)

V. CONCLUSIONS

To provide the high current consumed by lots of electronic loads on electrical vehicle, this paper designs a converter composed of three parallel PSFB DC-DC converters. The design procedures of parameters of the main circuit and controller are presented. The main circuit can realize ZVS. Additional resonant inductor can help to keep ZVS when the load is not large enough. The loss of duty cycle is considered when modelling. The peak current mode control can avoid magnetic saturation of transformer. The experimental results show that the even current sharing is achieved between the three modules. The overall temperature of the converter is within a reasonable range, which indicates the rationality of the design.

REFERENCES

- [1] J. A. Sabate, V. Vlatkovic, R. B. Ridley, F. C. Lee and B. H. Cho, "Design considerations for high-voltage high-power full-bridge zero-voltage-switched PWM converter," Fifth Annual Proceedings on Applied Power Electronics Conference and Exposition, Los Angeles, CA, USA, 1990, pp. 275-284, doi: 10.1109/APEC.1990.66420.
- [2] H. Aksoy and M. T. Aydemir, "Comparison of zero voltage switching phase-shifted PWM full bridge DC-DC converter topologies," 2015 Intl Aegean Conference on Electrical Machines & Power Electronics (ACEMP), 2015 Intl Conference on Optimization of Electrical & Electronic Equipment (OPTIM) & 2015 Intl Symposium on Advanced Electromechanical Motion Systems (ELECTROMOTION), Side, 2015, pp. 818-824, doi: 10.1109/OPTIM.2015.7427028.
- [3] A. F. Bakan, N. Altıntaş and İ. Aksoy, "An Improved PSFB PWM DC-DC Converter for High-Power and Frequency Applications," in IEEE Transactions on Power Electronics, vol. 28, no. 1, pp. 64-74, Jan. 2013, doi: 10.1109/TPEL.2012.2196287.
- [4] Y. Tang, Y. Wu, Z. Chen, C. Zhang and W. Hu, "Hybrid mode control for wide range soft-switched full-bridge converter with auxiliary parallel inductor networks," in IET Power Electronics, vol. 12, no. 7, pp. 1670-1678, 19 6 2019, doi: 10.1049/iet-pel.2018.6104.
- [5] A. Mallik and A. Khaligh, "Variable-Switching-Frequency State-Feedback Control of a Phase-Shifted Full-Bridge DC/DC Converter," in IEEE Transactions on Power Electronics, vol. 32, no. 8, pp. 6523-6531, Aug. 2017, doi: 10.1109/TPEL.2016.2616033.
- [6] S. Lee, J. Lee, U. A. Khan and J. Park, "Novel Switching Control Method for Synchronous Rectifier of Phase-Shifted Full-Bridge Converter in Light-Load Conditions," 2019 IEEE Energy Conversion Congress and Exposition (ECCE), Baltimore, MD, USA, 2019, pp. 1408-1413, doi: 10.1109/ECCE.2019.8912223.

- [7] C. Zhao, X. Wu, P. Meng and Z. Qian, "Optimum Design Consideration and Implementation of a Novel Synchronous Rectified Soft-Switched Phase-Shift Full-Bridge Converter for Low-Output-Voltage High-Output-Current Applications," in IEEE Transactions on Power Electronics, vol. 24, no. 2, pp. 388-397, Feb. 2009, doi: 10.1109/TPEL.2008.2005269.
- [8] L. Hua, J. Guo, X. Jing, N. Mi, R. Chung and S. Luo, "Design considerations for secondary side synchronous rectifier MOSFETs in Phase Shifted Full Bridge Converter," 2013 Twenty-Eighth Annual IEEE Applied Power Electronics Conference and Exposition (APEC), Long Beach, CA, 2013, pp. 526-531, doi: 10.1109/APEC.2013.6520260.
- [9] Y. Sun and B. Jiao, "Design of a soft-switched phase-shift full bridge converter," 2016 3rd International Conference on Systems and Informatics (ICSAI), Shanghai, 2016, pp. 230-234, doi: 10.1109/ICSAI.2016.7810959.
- [10] N. Vazquez and M. Liserre, "Peak Current Control and Feed-Forward Compensation for the DAB Converter," 2019 IEEE International Conference on Industrial Technology (ICIT), Melbourne, Australia, 2019, pp. 685-690, doi: 10.1109/ICIT.2019.8755238.
- [11] M. Hallworth and S. A. Shirsavar, "Microcontroller-Based Peak Current Mode Control Using Digital Slope Compensation," in IEEE Transactions on Power Electronics, vol. 27, no. 7, pp. 3340-3351, July 2012, doi: 10.1109/TPEL.2011.2182210.

Energy Storage, Fuel Cell and Electric Vehicle Technology

Cheng K.W.E.

Power Electronics Research Centre, Department of Electrical Engineering
The Hong Kong Polytechnic University, Hong Kong
E-mail: eechengs@polyu.edu.hk

Abstract – The energy storage components include the Li-ion battery and super-capacitors are the common energy storage for electric vehicles. Fuel cells are emerging technology for electric vehicles that has promising high traveling distance per charge. Also, other new electric vehicle parts and components such as in-wheel motor, active suspension, and braking are emerging recently to upgrade the vehicles’ performance. In this tutorial, the above topics are discussed and an outlook on future vehicles is highlighted. The tutorial paper is suitable for researchers or engineers with a deep knowledge of electric vehicles and is also suitable for someone new to the field.

Keywords: Energy storage, Electric Vehicles, Redox flow battery, super-capacitor, fuel cell, active suspension, in-wheel motor, configurable EV, ABS.

I. INTRODUCTION

The critical components of an Electric Vehicle are the battery and the motor drive. Energy storages such as batteries and super-capacitors are now the major energy storage units. The energy sources like fuel cells and flow batteries are also getting popular and are promising energy storage for future devices. Thanks to the hydrogen economy, the coming new fuel with zero carbon will be a trend. Energy cell packaging is now in a new direction. The use of energy cells to integrate with the vehicle body has been reported and suggests good potential for energy management. The energy management and balancing technique is now a necessary component to manage the energy cells. Besides the energy storage and the traction motor and drives, there are numerous motors and actuators used in modern electric vehicles. They are located in various positions of a vehicle to replace the conventional mechanical and hydraulic system. They may include an active suspension system to replace the conventional hydraulic system. The In-wheel motor is based on integrating the motor and wheel into a single unit that increases the power density and presents a real 4-wheel drive. The skid steering can, therefore, be realized. Also, the E-anti-lock braking (ABS) is an all-electric braking system and replaces the conventional hydraulic system in ABS. In this paper, the energy and fuel technology are reviewed and the new electric vehicle technology is examined and highlight future vehicle development.

II. BATTERY TECHNOLOGY

A. Common battery

In general, energy storage for all feasible energy storage for an electric vehicle could be electrochemical, electrostatic, and chemical types. Fig 1 shows an

illustration. Basically, the energy storage or fuel can be classified into Electrochemical – conversion between electricity and chemical energy, electrostatic – conversion between electricity and static electric/magnetic field, mechanical – conversion between mechanical energy and electric energy, chemical – conversion from thermal chemical to electricity.

In the past, using hydrogen Internal combustion engine (ICE) has been developed because of its zero emission, but it is gradually replaced by hydrogen fuel cell .

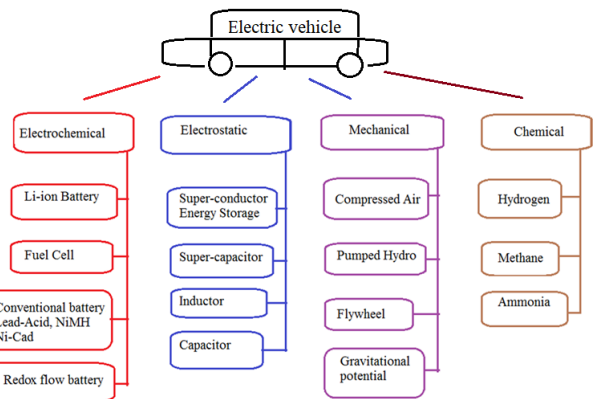


Fig 1: Fuel and energy storage for electric vehicles.

The battery is now using Li-ion as the common energy storage because its technology is ready and quite mature. Table 1 shows the typical energy storage for common cells:

Table 1: Common Lithium ion battery characteristics

	LiCoO_2	LiMnO_4	$\text{LiNi}_{1/3}\text{Mn}_{1/3}\text{Co}_{1/3}\text{O}_2$	LiFePO_4	LiTiO_4	$\text{LiNi}_{0.8}\text{Co}_{0.15}\text{Al}_{0.05}\text{O}_2$
Specific Energy (Wh/kg)	180	100	180	140	100	160
Number of Cycles (life time)	1000	1000	1000	2000	10000	1000
Cell voltage (V)	3.7	3.8	3.8	3.2	2.2	3.7

Besides the above common batteries, other higher performance battery such as Lithium-Sulphur [1] or Li-Oxygen battery [2] has promising performance and may be an option for a future vehicle. Fig 2 shows an illustration of different energy storages. The fuel cell has

a good potential for the future long-range vehicle, and super-capacitor is suitable for high power short-range vehicle.

B. Redox flow battery

Reduction-oxidation (Redox) flow battery is another possible battery for electric vehicles because its energy storage is based on the electrolyte [3]. Therefore the charging is similar to adding liquid fuel which is the electrolyte to a vehicle’s tank. Fig 3 shows the configuration. The diagram shows a popular diagram for vanadium Redox flow battery, but other flow battery using other technology such as Zinc-bromide is also common.

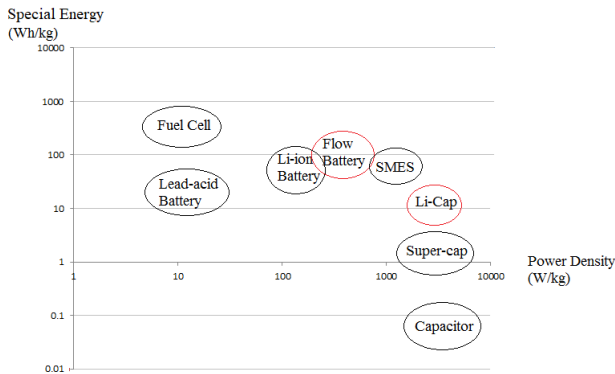


Fig 2: Special energy of various energy storage or fuel

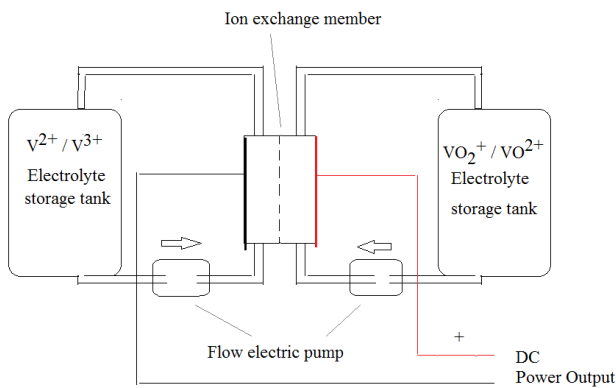


Fig 3: A schematic of redox flow battery (with vanadium)

III. BATTERY MANAGEMENT SYSTEM

Battery management system (BMS) is the basic protection and monitoring devices for all battery vehicles. It allows the estimation or the measurement of the State of Charge (SoC), State of Health (SoH), cell equalization, and communication and control, with other vehicle parts and vehicle control unit (VCU). SoC varies with the current, temperature, and cell voltage, therefore the estimation of SoC cannot be done by Coulomb-counting, but predictive modeling is needed.

A. Passive Cell Equalization

The common cell balancing is using passive balancing in which the over-charge cell is discharged by a resistor and hence the balancing is not adaptive and it is more like overvoltage protection [4].

B. Active Cell Equalization

The active version is using inductors or capacitors to temporary to store the energy and use it to transfer energy from over-voltage cell to under-voltage cell. Fig 4 shows the two typical methods:

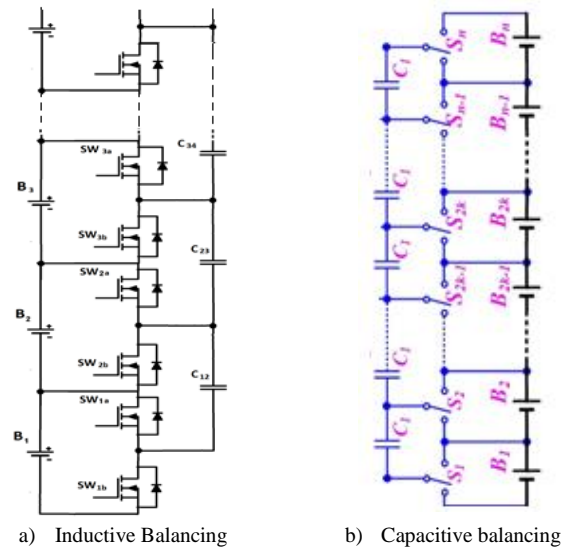


Fig 3: Typical Cell Equalization scheme

IV. BODY INTEGRATED SUPER-CAPACITOR FOR VEHICLES

A. Body integration concept

The new concept of energy storage is not to place all the energy storage in a single compartment of location, such as in the back, of the bottom of a vehicle, but to distribute the energy storage over different vehicle parts. The door, wing, boot, or chassis can be part of the body integrated energy storage location. The idea is to integrate the package of the super-capacitor and the body part to reduce the unnecessary package or enclosure. Of course, the location is special and it must be selected so that it does not affect the vehicle operation and even under accident, it is safe proof. This concept is called distributed energy storage for vehicles. The design allows energy storage can power electronics units locally and reduce power distribution and loss. It also allows the future design of configurable vehicles. Fig 5 shows the concept:



Fig 5: Distributed energy storage concept for vehicles.

B. Super-capacitor and battery management system,

The management for both supercapacitor and battery is shown in Fig 6. It consists of the battery management unit (BMU) and the Super-capacitor management unit (SMU) to measure the information from each battery and supercapacitor module respectively. Their information is communicated to the master control unit through the CAN bus.

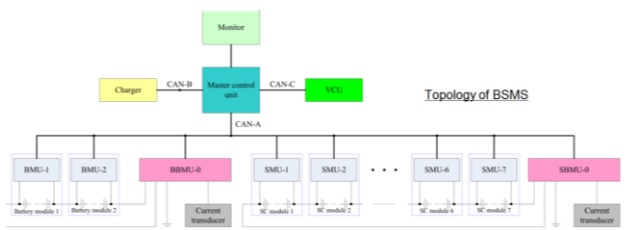


Fig. 6: Super-capacitor and battery management system

IV. FUEL CELL VEHICLE

A. World metal resources

Vehicles using Lithium-ion battery has a potential problem. The world production of Lithium is very low as compared with other metals. The first is iron and the second is aluminium. The production quantity of lithium is close to silver or gold. That means it is precious and the source is limited. Fig 7 shows the chart of the metal world production. Therefore using Lithium as energy storage will impose a major issue in coming years.

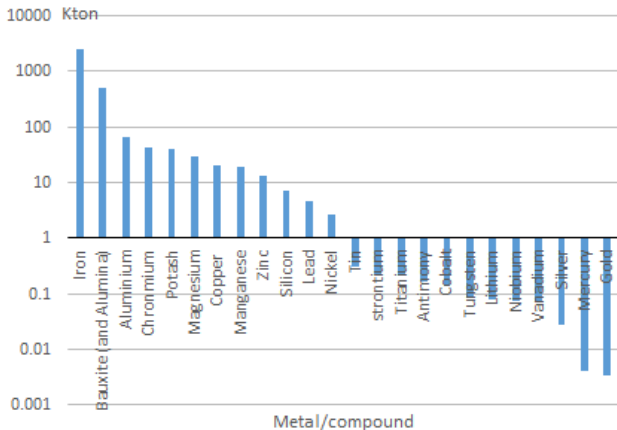


Fig 7: World production of major metals per year.

The Aluminium and zinc's prices in the last 5 years are very stable and therefore using Aluminium and zinc as the fuel such as Aluminium and zinc fuel cell, the potential benefit is much better than Lithium or Cobalt. The price of Aluminium in the last 5 years varies between USD 360 to 510 / ton and Zinc's price varies between USD310 to 750 / ton [5]. The variation is 1.7 times and 2.4 times for Aluminium and Zinc between the highest and lowest price.

B. Effect to battery materials

However, for Cobalt and Lithium which are the major metal components for Li-ion batteries, the price varies significantly in the last 5 years. Cobalt's price varies from USD 4500 to 20000 / ton whereas Lithium's price varies between USD 5000 to 22000 per ton [6]. They represent the variation of 4.4 times between the highest and lowest price.

C. Fuel cell vehicle

The design of any fuel cell vehicle needs energy storage such as battery and supercapacitor in order to ensure the dynamic energy during braking and deceleration can be stored because fuel cell cannot convert electrical current to fuel. Fig 8 shows the typical design of a fuel cell vehicle. The fuel shown can be any hydrogen carrier fuel that may be cracker or purifier. However, if it is metal fuel, then it is directly inserted into the Fuel cell reactor.

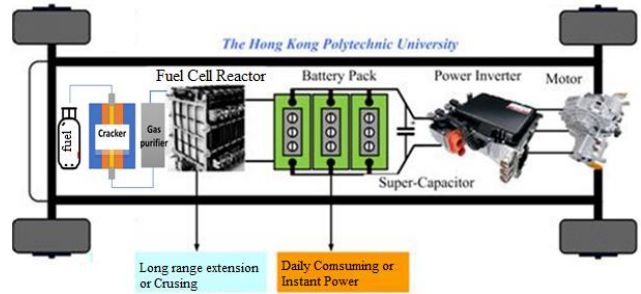


Fig 8. Fuel cell vehicle configuration.

V. IN WHEEL MOTOR

The integration of the motor to the wheel is so-called the in-wheel motor. The design criteria are that the motor must have high power density so that it can be included in the wheel and it is, therefore, direct-drive and there is no mechanical linkage such as transmission, gearbox, clutch, and shaft and thus the efficiency is high. The wheel speed is designed to be low and the torque must be large. The motor should have vibration tolerance as well. Fig 9 shows the development of an in-wheel motor using switched reluctance motor technology so that the permanent magnet can be eliminated [7]



Fig 9: In-wheel motor with the cover open.

VI. ACTIVE SUSPENSION

Instead of using hydraulic suspension which is slow and not adaptive, using a linear motor to replace the conventional suspension is a future design for vehicles [8]. It provides high dynamic performance and its response is much faster. Fig 10a shows the design of an active suspension which forms a linear actuator or motor. It consists of a translator which is the moving part to control the sprung mass of the vehicle to move and the stators consist of a number of phases that is fixed on the four

wheels. The active suspension is controlled to reduce heave and vibration.

Fig 10b shows the sample of the active suspension which its shape is square. Another shape is available with different designs of the translator and stators. Another advantage of the active suspension is that its vibration energy that is wasted in the conventional hydraulic suspension is wasted, whereas the present system can recover the energy and return to the battery.

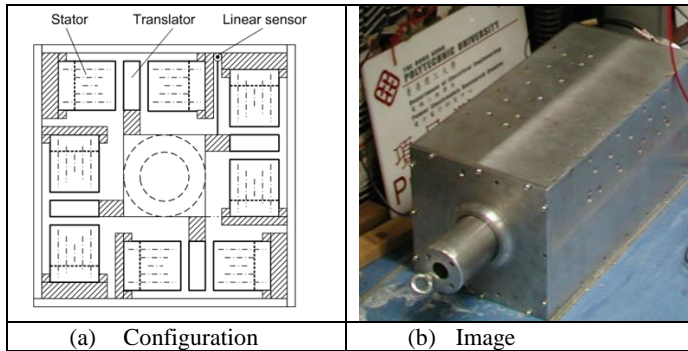


Fig 10: The Active suspension using switched-reluctance Technology

VII. ALL ELECTRIC ANTI-LOCK BRAKING SYSTEM

The mechanical disk braking basically relies on a hydraulic or pneumatic system which is not reliable and needs maintenance. The recent research using force motor to replace the mechanical system is a preferred design. It has high dynamic performance [9] and can control the optimized slip as shown in Fig 11. Fig 12 shows how the force motor connected to the wheel.

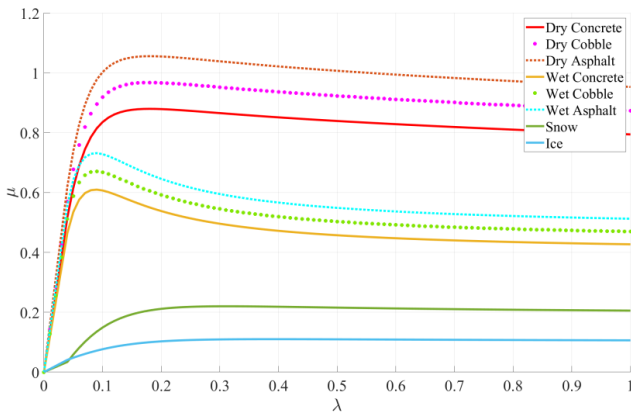


Fig 11: Relationship between Road friction coefficient and slip

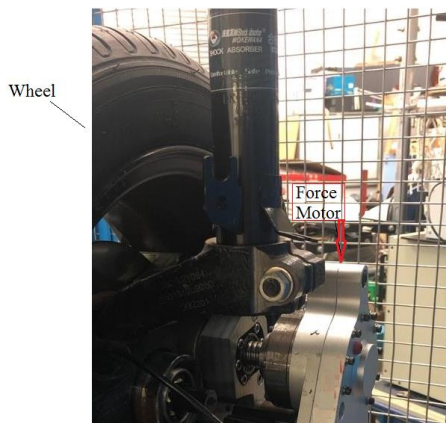


Fig 12: E-ABS testing in the laboratory

VIII. WIRELESS POWER TRANSFER FOR VEHICLES

The conductive charging has a few issues that are not welcome by users. For example, the cable connection is bulky, worry of electrical shock, concerned humid of raining season, connection aging, compatibility of socket and plug and standardization. The wireless power transfer is usually applied to a charger which can be briefly divided into stationary and move-and-charge. The coils between the primary and second are coupled inductors that form the air-gapped transformer. The converter associated with the coupled inductor is the bridge resonant converter as shown in Fig 13. Fig 14 shows the coils and converter development which is technology for move-and-charge design [10].

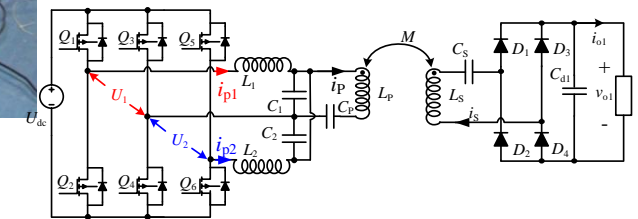


Fig 13: Coupled inductor used in resonant power converter.

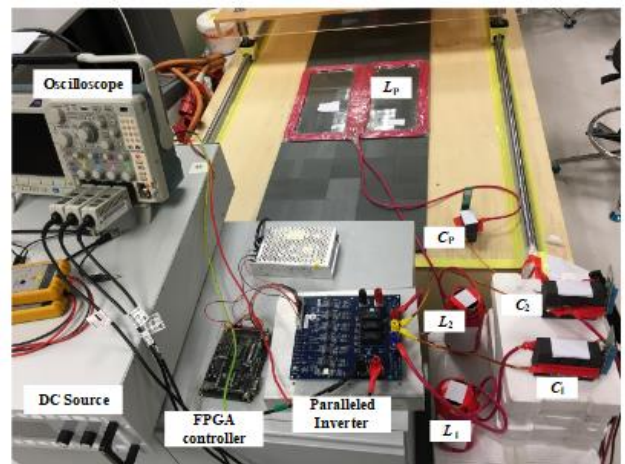


Fig 14: Implementation of the move and charge for vehicles.

IX. FUTURE VEHICLES AND CONCLUSION

Future vehicle design should meet the requirement of long traveling distance per charge. The maintenance is expected to be low and also the control is simple and has good and smart sensing and monitoring, as well as fault tolerance. Therefore autonomous driving is one of the present and future features of the electric vehicles. All the conventional mechanical and hydraulic systems will be replaced by electric motors or actuators so that diagnosis is all computerized and traceable. Therefore the dynamics response of the vehicle is fast.

The technologies of power electronics, magnetics, motors, smart sensors, and smart control are the tools for electric vehicle development. Other special applications of vehicles will also be in demand such as configurable vehicles so that a vehicle can change its shape or function when needed.

ACKNOWLEDGMENT

The author gratefully acknowledges the support of the researchers in Power Electronics Research Center of the university.

REFERENCES

- [1] Abbas Fotouhi; Daniel J. Auger; Karsten Propp; Stefano Longo, "Electric vehicle battery parameter identification and SOC observability analysis: NiMH and Li-S case studies", IET Power Electronics, 2017, Volume: 10, Issue: 11
- [2] Yulin Cao; Siu Wing Or, "Enhanced Cyclability in Rechargeable Li-O₂ Batteries Based on Mn₃O₄ Hollow Nanocage/Ketjenblack Catalytic Air Cathode", IEEE Transactions on Magnetics, 2016, Vol. 52, Issue: 7.
- [3] Maria Skyllas-Kazacos^{1,2,*,y}, George Kazacos², Grace Poon¹ and Hugh Verseema, "Recent advances with UNSW vanadium-based redox flow batteries", International Journal of Energy Research, 2010; 34:182–189
- [4] K.W.E.Cheng, "Review of battery management systems for electric vehicles", Chapter 12 of "Energy Systems for Electric and Hybrid Vehicles", IET, Aug 2016, ISBN: 978-1-78561-008-0.
- [5] Nicholas LePan, All the world's metal and Minerals in a Visualization, Visual Capitalist, Mar 1, 2020. <https://www.visualcapitalist.com> (Last Access: 1 Dec 2020)
- [6] Mining.com, <https://www.mining.com/markets/commodity/> (Last Access: 1 Dec 2020)
- [7] X. D. Xue, K. W. E. Cheng, T. W. Ng, and N. C. Cheung, "Multi-Objective Optimization Design of In-Wheel Switched Reluctance Motors in Electric Vehicles", IEEE Trans Industrial Electronics, Vol. 57, Issue: 9, 2010, pp. 2980 – 2987
- [8] J.K.Lin, K.W.E.Cheng, "Active Suspension System Based on Linear Switched Reluctance Actuator and Control Schemes", IEEE Transactions on Vehicular Technology, Vol. 62, Issue: 2, 2013, pp. 562 – 572
- [9] Jinhong Sun, Xiangdang Xue and Ka Wai Eric Cheng, "Fuzzy Sliding Mode Wheel Slip Ratio Control for Smart Vehicle Anti-Lock Braking System", Energies, 2019, 12, 2501; doi:10.3390/en12132501
- [10] Yong Li; Jiefeng Hu; Xiaofei Li; Ka-Wai Eric Cheng, "A Flexible Load-Independent Multi-Output Wireless Power Transfer System Based on Cascaded Double T-Resonant Circuits: Analysis, Design and Experimental Verification", IEEE Transactions on Circuits and Systems I: Regular Papers, Vol 66, No 7, July 2019, pp 2803-2816.

Study and Development of Mixed Repurposing EV Battery System for Stationary Energy Storage Applications

Y.C. Fong, D.H. Wang, J. Mei, S. Raghu Raman and K.W.E. Cheng
 Power Electronics Research Centre, Department of Electrical Engineering
 The Hong Kong Polytechnic University
 Hung Hom, Kowloon, Hong Kong
 E-mail: yc-chi.fong@connect.polyu.hk

Abstract – This paper presents a case study of developing a stationary battery energy storage system (ESS) with a combination of used batteries from different electric vehicles (EVs). The batteries having nonidentical specifications, dismantled from two models of retired EVs with varied conditions, have been characterized. The state of health and the expected electrical performance of these repurposed batteries from EVs are analyzed and compared. A modular battery ESS with dual feed configuration is developed to strike a balance between reliability, performance and the cost of implementation. The modular approach allows flexibility in capacity and voltage level manipulation, as well as mitigates the efforts of battery replacement. The construction and key components in the systems are illustrated and explained. A simulation study has been performed which explores the effects of varied battery profiles and combinations to system performance. This work provides insights on designing and operating sustainable stationary ESS with mixed repurposed cells.

Keywords: Second life battery, batter recycling, electric vehicle, Battery repurposing.

I. INTRODUCTION

The penetration of electric vehicles (EVs) has been rapidly grown since last decade. From 2014 to 2019, the accumulative number of EVs produced in the world is over 4.5 million [1]. At present, over 500 GWh of EV batteries have been deployed worldwide, and the total capacity produced in each year are projected with a compound annual growth rate of about 25% in the coming decades [1]. In general, the lifespan of a battery EV is mainly limited by the battery cells, which normally last for about 8 to 15 years depending on the usage profile and battery technology. On one hand, the EVs offers an alternative transportation solution with zero road emission; on the other hand, the production and disposal of the batteries creates extra burden to the environment. Currently, the EV batteries are dominated by the Li-ion technology which provides sufficient power and energy density for traction power and driving range. Although the toxic metal content is lower compared to other battery technologies such as the lead-acid and nickel-cadmium based, without a proper treatment, cobalt, nickel, and other kinds of metals in the disposed lithium batteries would contaminate the ecosystem. In view of the increasing number of EVs retiring from the road, tackling of end-of-life EV batteries has become an emerging matter for both industry and authority. As a buffer to economically well-established recycling system, as well as to maximize the life-cycle value of the high-performance EV batteries, repurposing them into other applications is

considered a promising way to relief the environmental impact of the end-of-life EV batteries. pack design.

Having about 60 to 80% state-of-health in general, the used EV batteries may no longer be suitable for automobiles, but still be capable of serving stationary energy storage for utilities, as well as other commercial and residential applications. For example, [2] presents a community energy storage system which provides grid ancillary services to local area; [3] and [4] demonstrates the feasibility of used EV batteries in both off-grid and grid-tied renewable systems.

Along with the battery technology development, there are variety of battery chemistries available in the market as well as deployed to different EVs. A second-life application capable of mixed batteries would greatly improve the availability and sustainability for the deployment of used EV batteries. This works presents the use of mixed repurposing EV battery into a back-up power supply for building applications. A battery energy storage system (BESS) with two types of used EV batteries is developed. A case study on different system composition is also conducted, which explores the design consideration of a mixed BESS.

II. OVERVIEW OF THE PROPOSED SYSTEM

A battery energy storage system has been developed employing two different models of used EV batteries. The system configuration of the BESS is depicted in Fig. 1. The BESS consists of two strings of battery modules connected in-series via blocking diodes. The battery strings are constituted by series and parallel combinations of battery modules to form the desired capacity and voltage. Each of the modules is rated at 30 V and formed by eight sorted Li-ion battery cells connected in-series. With a 6S module configuration, the BESS has a total DC bus voltage rated at 180 V. The BESS has dedicated ports for charging and discharging. The charging port is connected to a charger integrating PV generation and utility mains; the discharging port is supplying to AC loads at 50 Hz 380 V through an inverter. With this configuration, the parallel strings provide additional redundancy in case of battery failure. Besides, the modular structure makes the replacement of battery much easier comparing to a single-pack design.

The system is constituted by the used batteries dismantled from Mitsubishi i-MiEV and Renault Fluence Z.E. (Fig. 2).

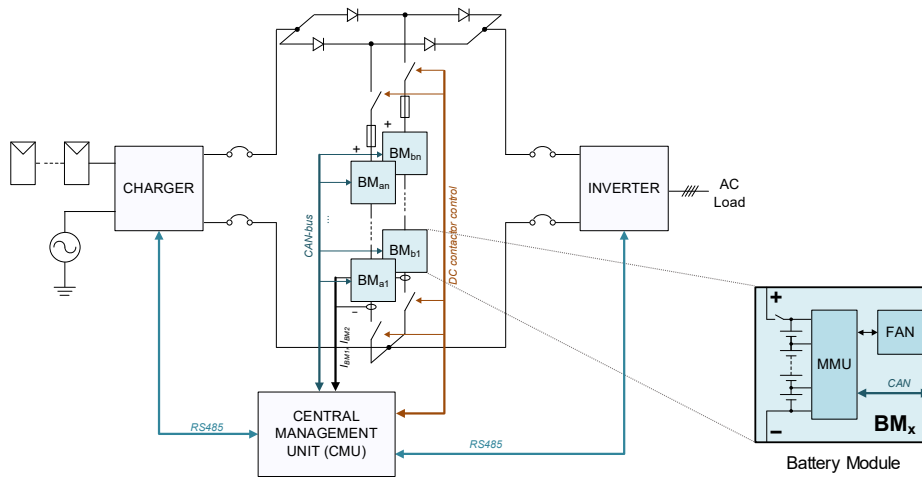


Fig. 1: The proposed energy storage system based on mixed repurposed EV batteries.

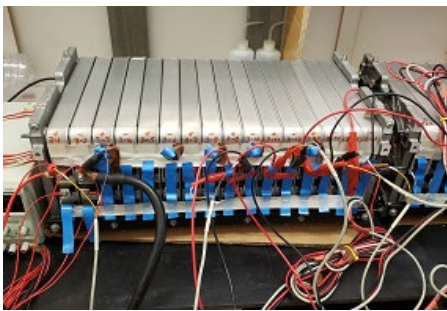


Fig. 2: The used EV batteries dismantled from a Renault Fluence Z.E. and placed on a test bench for measurement.

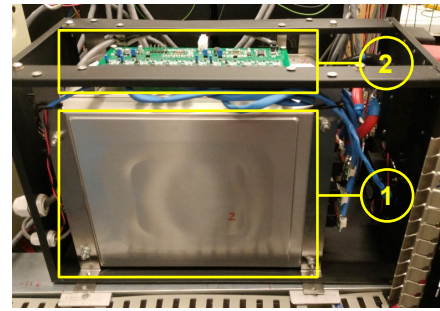


Fig. 3: Side view of an open-up battery modules; (1) the battery cells; (2) the module management unit (MMU).

A picture of the battery module prototype is depicted in Fig. 3 and 4. In each battery module, there is a manual switch accessible on the exterior of the chassis. When handling or replacing the battery module, the switches on the upper and lower, as well as the handling modules are opened to ensure that the circuit is cut-off. This improves the safety of battery installation and maintenance. Each of the modules is conditioned by a module management unit (MMU) which measures the voltage across each cell and the temperature of the cell terminals. The passive balancing switches in the MMU are controlled based on the cell voltage threshold and measured cell voltage difference. The cooling fans installed in the modules are also managed by the MMU based on the thermal condition. The voltage and temperature measurements, thresholds, as well as the operating status of the MMU are communicated to the central management unit (CMU) via an isolated Controller Area Network-bus (CAN-bus). The CMU collects the operating status of the battery modules via the CAN-bus, and controls the DC contactors of the battery strings accordingly. The CMU also monitors the voltage, current and insulation of the DC bus. Meanwhile, the CMU coordinates with the charger and inverter to monitor and manages the charge and discharge status of the BESS.

III. MEASUREMENTS AND ANALYSIS OF USED EV BATTERIES

In this study, the used batteries from two models of EVs are examined. After visual inspection on any signs of visible damage or cell failure such as electrolyte leakage and obvious swell. The terminal voltage of each cell under idle

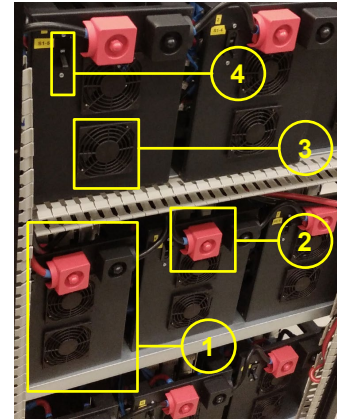


Fig. 4: A photo of the prototype; (1) a battery module; (2) module connection terminals; (3) cooling fan; (4) switch.

state was measured, followed by a full discharge test at 0.2 C of the rated capacity to measure the residual charge. These tests help screening unusable cells quickly at an early stage. After screening, the cells are sorted based on the analyzed results of the remaining capacity and the internal resistance. The measurements of the used battery dismantled from a retired Mitsubishi i-MiEV are shown in Fig. 5. The vehicle has been made full use of in its service for over 7 years with a total mileage of about 75,000 km. The battery cells inside the i-MiEV were LEV50 NMC [5] cells, with a rated capacity of 50 Ah, developed by GS-Yuasa. The measured terminal voltage of the cells when arrived was about 3.97 V with a range of around 100 mV. The remaining capacity of the used LEV50 cells with a charging constant voltage setting of 4.1 V and discharging

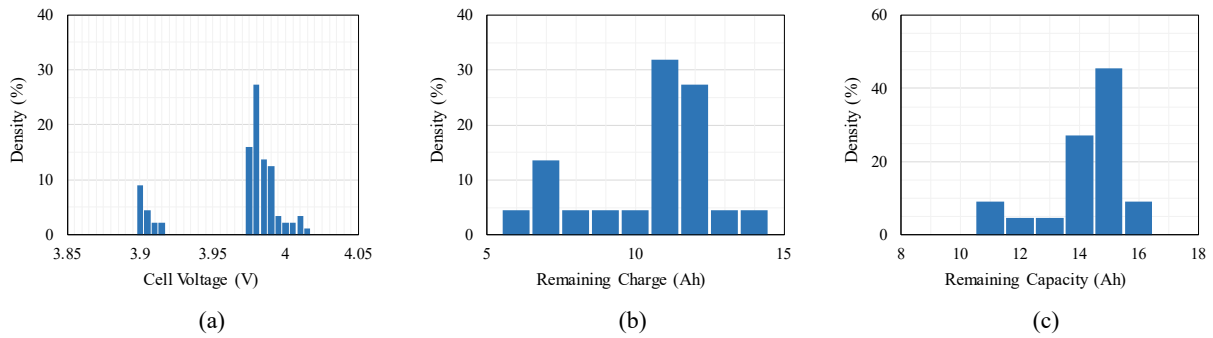


Fig. 5: Measurements and distribution of the used battery samples of LEV50 dismantled from a retired Mitsubishi i-MiEV. (a) Open-circuit voltage of the cells when arrived; (b) the residual charge in each of the cells; (c) the remaining available capacity.

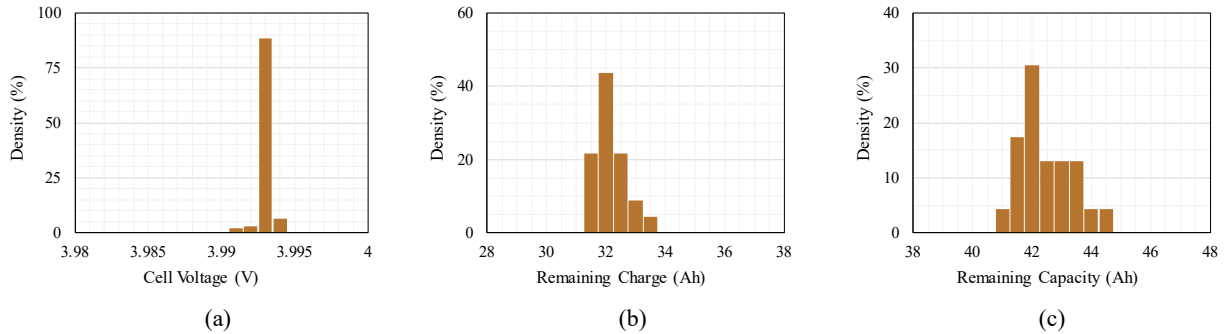


Fig. 6: Measurements and distribution of the battery samples from an end-of-service Renault Fluence Z.E. (a) Open-circuit voltage of the cells when arrived; (b) the residual charge in each of the cells; (c) the remaining available capacity.

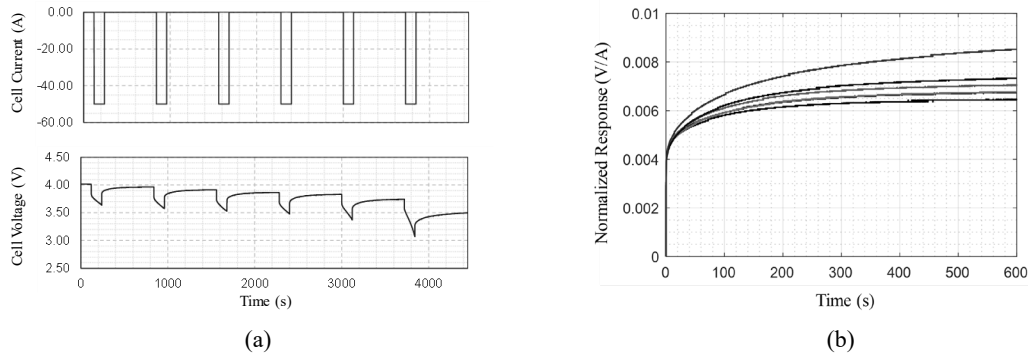


Fig. 7: The terminal voltage measurements of the used LEV50 cells under load current steps and the dynamic voltage response. (a) Measurements of cell voltage along with the load current steps; (b) the normalized dynamic cell voltage response to unit current step at different SOC.

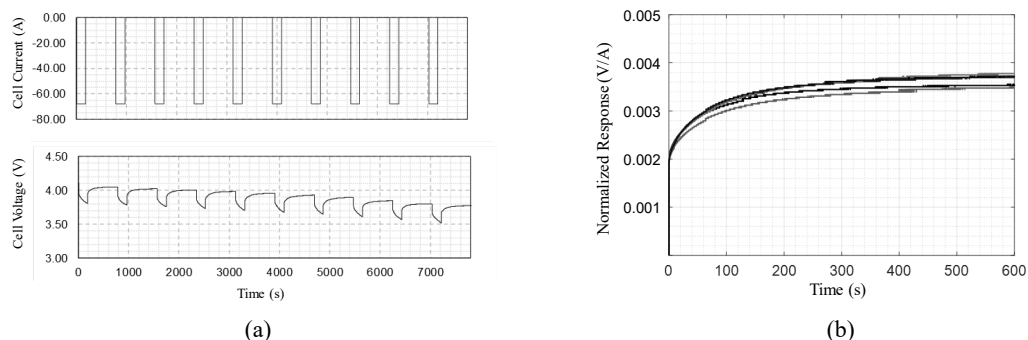


Fig. 8: The terminal voltage measurements of the used LMO cells from Fluence Z.E. under load current steps and the dynamic voltage response. (a) Measurements of cell voltage along with the load current steps; (b) the normalized dynamic cell voltage response to unit current step at different SOC.

cutoff voltage of 2.75 V was approximately 14 Ah. This is equivalent to 28 % state-of-health.

Similarly, the used LMO [6] cells from an end-of-service Renault Fluence Z.E. were examined. The cells dismantled from the Fluence Z.E. were at a healthier condition and

uniformity. As depicted in Fig. 6, the cells terminal voltage was about 3.99 V having a total difference of within 5 mV. The average residual charge and capacity were approximately 32 Ah and 42 Ah, respectively. This is equivalent to an average SOH of 62% compared to the rated capacity of 68 Ah.

Table 1: Fitted circuit parameters of the used cells under different SOC

Mitsubishi i-MiEV					
SOC	Resistance (Ω)			Capacitance (F)	
	R_0	R_1	R_2	C_1	C_2
0.80	0.00270	0.00199	0.00173	682	58496
0.66	0.00289	0.00185	0.00197	938	57687
0.52	0.00291	0.00179	0.00205	1037	55951
0.38	0.00306	0.00172	0.00224	1349	51611
0.24	0.00324	0.00156	0.00250	2433	51498
Renault Fluence Z.E.					
SOC	R_0	R_1	R_2	C_1	C_2
0.79	0.00204	0.00050	0.00099	36414	109669
0.63	0.00199	0.00065	0.00107	34497	127377
0.49	0.00202	0.00065	0.00113	38119	145466
0.31	0.00196	0.00062	0.00091	38760	177689
0.15	0.00198	0.00070	0.00104	34246	131444

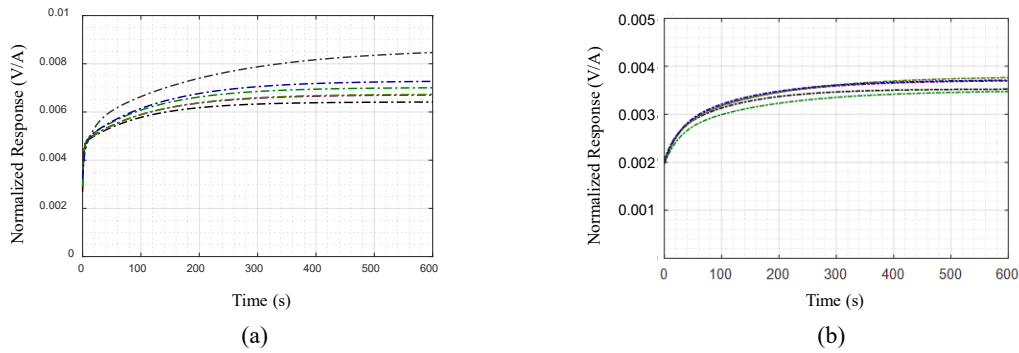


Fig. 9: Emulated step response of the used battery cells at different SOC values using the fitted electrical parameters. (a) the used LEV50 cell; (b) the LMO cells from used Fluence Z.E.

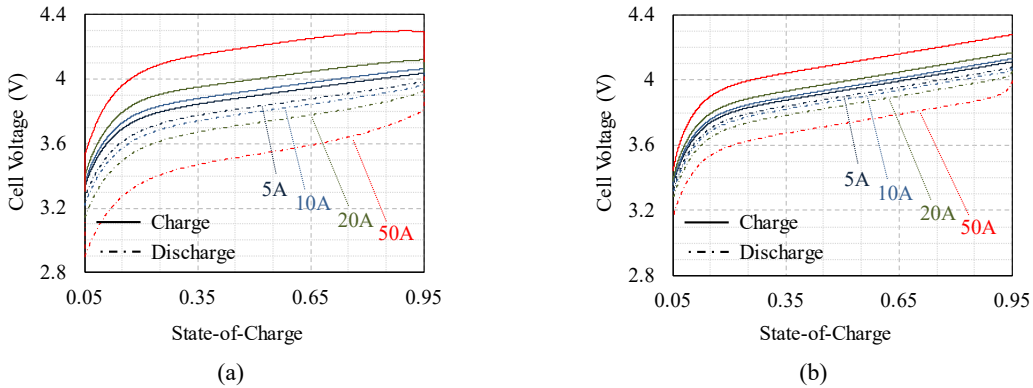


Fig. 10: Emulated charge-discharge characteristic of the used battery cells at different current. (a) the used LEV50 cell; (b) the LMO cells from used Fluence Z.E.

The electrical characteristic of the used cells was analyzed according to the measured voltage response to the applied load current step (Fig. 7 and 8). The dynamic responses of the cell voltage at different state-of-charge are normalized and modelled by a second order equivalent circuit model (1).

$$V_B = V_{OCV} + I_B [R_0 + R_1 (1 - e^{-\frac{-t}{R_1 C_1}}) + R_2 (1 - e^{-\frac{-t}{R_2 C_2}})] \quad (1)$$

where V_B and I_B are the terminal voltage and current of the cell, respectively. V_{OCV} is the internal cell voltage represented by an ideal SOC-dependent voltage source. R and C are the equivalent internal circuit parameters

representing voltage drop loss and time constant.

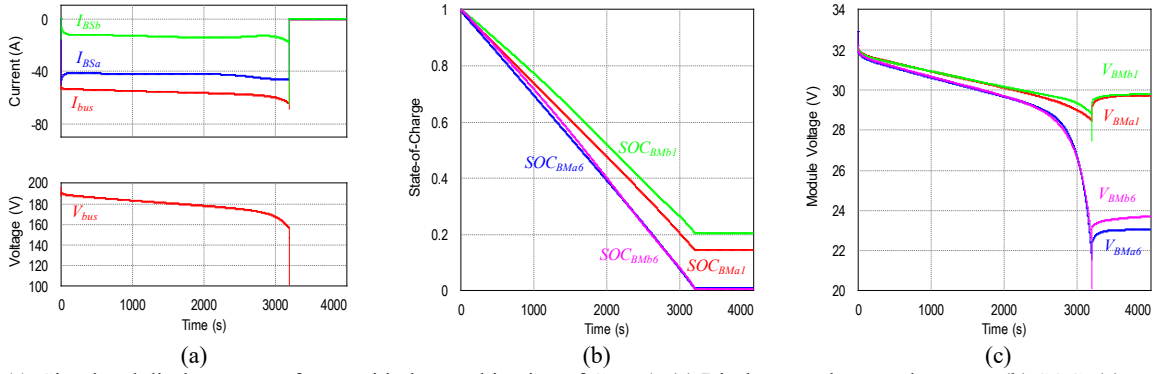
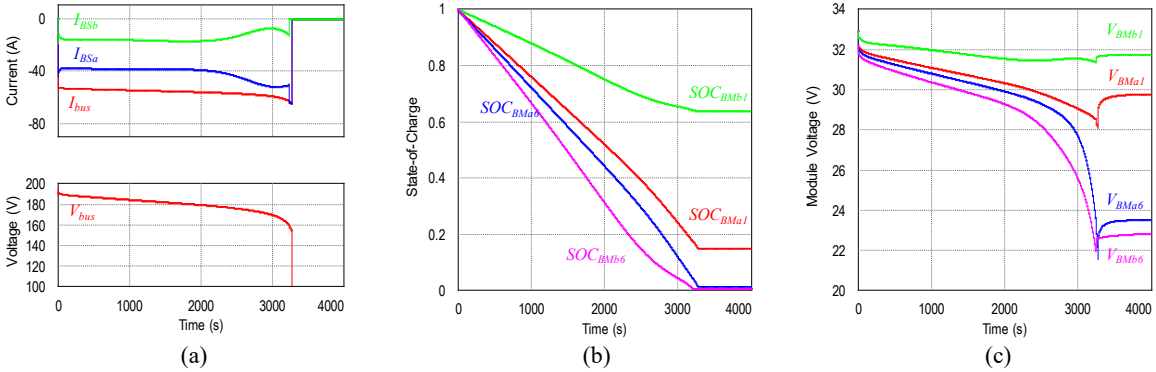
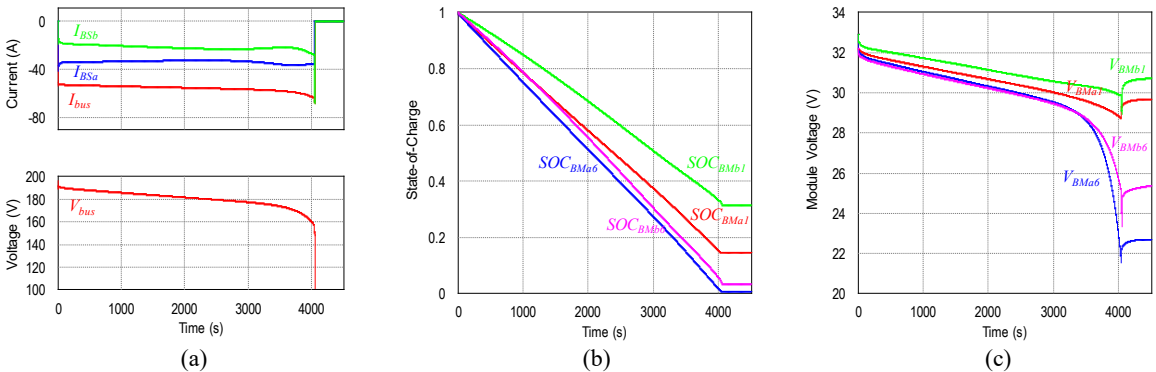
The measurements of the responses of the used battery cells could be fitted with the parameters shown in Table 1, which gives emulated responses of as depicted in Fig. 9. By putting the fitted parameters into the emulated battery models, the charge-discharge profiles of the two types of used battery under constant current charging and discharging at different current values are derived as Fig. 10. This gives an estimation on the cycle energy efficiency ranging from 84.3% at 50 A to 98.2% at 5 A for the used LEV50 cells of 28% SOH; and 91.1% to 99.1% in the same current range for the used cell from Renault Fluence Z.E.

Table 2: Modules available for deployment in the simulated mixed BESS

Mitsubishi i-MiEV		Renault Fluence Z.E.	
Module	SOH	Module	SOH
BM _{M1}	0.30	BM _{R1}	0.65
BM _{M2}	0.28	BM _{R2}	0.63
BM _{M3}	0.26	BM _{R3}	0.61
BM _{M4}	0.26	BM _{R4}	0.61
BM _{M5}	0.25	BM _{R5}	0.58
BM _{M6}	0.24	BM _{R6}	0.56
BM _{M7}	0.23	BM _{R7}	0.53
BM _{M8}	0.21	BM _{R8}	0.50

Table 3: Combinations of battery modules in different cases

Case-1	
String-A	String-B
BM _{R1} , BM _{R2} , BM _{R3} , BM _{R4} , BM _{R5} , BM _{R6}	BM _{M1} , BM _{M2} , BM _{M3} , BM _{M4} , BM _{M5} , BM _{M6}
Case-2	
String-A	String-B
BM _{R1} , BM _{R2} , BM _{R3} , BM _{R4} , BM _{R5} , BM _{R6}	BM _{R7} , BM _{R8} , BM _{M1} , BM _{M2} , BM _{M3} , BM _{M4}
Case-3	
BM _{R1} , BM _{R2} , BM _{R3} , BM _{R4} , BM _{R5} , BM _{R6}	BM _{R7} , BM _{R8} , BM _{M1} BM _{M8} , BM _{M2} BM _{M7} , BM _{M3} BM _{M6} , BM _{M4} BM _{M5} ,


Fig. 11: Simulated discharge waveforms with the combination of Case-1. (a) Discharge voltage and current; (b) SOC; (c) module voltages.

Fig. 12: Case-2. (a) Discharge voltage and current; (b) SOC; (c) module voltages.

Fig. 13: Case-3. (a) Discharge voltage and current; (b) SOC; (c) module voltages.

IV. SIMULATION STUDY

A case study on the effect of the variations in battery profiles and the combination of batteries in the mixed BESS has been performed with numerical simulation. The

simulation settings and parameters were designed referring to the system setting and the measured statistic on the used batteries. Based on the capacity measurements on the repurposing battery modules, the case study would be derived based on the available modules listed in Table 2. There are in total 16 modules, 8 modules with SOH ranged

from 0.21 to 0.30 from the i-MiEV and eight modules with SOH of 0.50 to 0.65 from the Fluence Z.E., available for building the two battery strings, String-A and String-B. The module combinations in different cases are shown in Table 3. In Case-1, the best six modules from the respective Fluence Z.E. and i-MiEV would be selected to form the two strings while the remaining are severed as spares for future replacement; in Case-2, all modules formed from Fluence Z.E. cells would be used, and the rest are filled by the i-MiEV modules with highest SOH; in Case-3, all modules are used, the i-MiEV modules with the highest and lowest SOH would be connected in parallel to form a capacity comparable to the Fluence Z.E. modules. In the simulation model, the battery strings were connected together via blocking diodes to discharge to a 10-kW constant power load. All battery modules were fully charged initially. The corresponding battery string would be switched-out when one of the corresponding cells touch the cut-off voltage of 2.75 V. The discharge operation of the BESS ends if the DC contactors of both battery strings are opened.

The simulated results are illustrated in Fig. 11 to 13. The DC bus voltage, V_{bus} , as well as the bus current, I_{bus} , and the respective string currents, I_{BSa} and I_{BSb} , are shown. Throughout the discharge operation, the DC bus voltage decreased from an initial value of 196.8 V to a minimum value of about 148.8 V, and the maximum bus current was 67.2 A. The initial dynamic load current was distributed among the two strings majorly dependent on the corresponding internal impedance. Then, both the capacity and voltage characteristic have significant on the current sharing. In Case-1, approximately 75% of the load current was allocated to the String-A with Fluence Z.E. cells. While in Case-3, the parallel i-MiEV modules effectively reduced the impedance and increased the capacity of String-B, the load current allocated to String-A was drop to 60%. Besides, the module voltages as well as the SOC of the highest and lowest SOH modules in the respective battery strings are captured. Due to a comparatively large difference in the SOH or the remaining capacities, both the charge and battery voltage diverged along with discharging. The imbalance was more distinct in Case-2 where the Fluence Z.E. and i-MiEV modules with significant capacity difference were mixed used in String-B. At the end of discharging operation, the Fluence Z.E. modules in String-B had roughly 64% of unused charge. The total available discharging capacity in this case was limited by the i-MiEV modules with lower SOH. In these three cases, the discharging operation ended at about 3200 s, 3272 s and 4050 s, respectively. This would be corresponding to total discharging capacity of 8.89 kWh, 9.09 kWh and 11.25 kWh with efficiency of 95.75%, 95.85% and 96.46% for Case-1, Case-2 and Case-3, respectively.

The case study suggests that parallel two low SOH modules in a mixed BESS could improve the overall available capacity and performance of the system. This provides insight in the operation design and replacement schedule. For example, the used battery cells with better condition could be allocated to String-A. While the modules in String-A are further aged, the old modules can be used in

parallel in String-B when a new batch of retired EV battery is available. The proposed replace schedule could make best use of the second-life EV batteries.

V. SUMMARY

This paper presents a case study on the development of the back-up power supply with mixed repurposing EV batteries for building applications. The spent batteries from Mitsubishi i-MiEV and Renault Fluence Z.E. with different conditions are deployed to the system. The measurements showed that the used NMC cells from the i-MiEV have SOH of about 30% while the SOH of the LMO cells dismantled from the Fluence Z.E. was around 60%. The batteries are considered thoroughly used in their first-life in EVs, while still able to delivery power at fair efficiency in their second-life in stationary applications. A simulation of various cases of combining mixed battery modules in different ways has been conducted. By designing a module composition such that the capacity of the series modules and the impedance among the parallel strings are sorted the performance of the mixed BESS can be optimized and the second-life of the EV batteries can be fully utilized with a two-tier operation arrangement. This offers a repurposing EV battery application with improved availability and sustainability.

ACKNOWLEDGMENT

The project development is financially supported by Electrical and Mechanical Services Department (EMSD) of the HKSAR. The authors wish to thank EMSD and Hongkong Electric Co. Ltd. for the donation of used EV batteries. The research is also supported by Power Electronics Research Centre (PERC) at the Hong Kong Polytechnic University.

REFERENCES

- [1] *Global EV Outlook 2020 – Analysis - IEA*. [Online]. Available: <https://www.iea.org/reports/global-ev-outlook-2020>.
- [2] O. C. Onar, M. Starke, G. P. Andrews and R. Jackson, "Modeling, controls, and applications of community energy storage systems with used EV/PHEV batteries," *2012 IEEE Transportation Electrification Conference and Expo (ITEC)*, Dearborn, MI, 2012, pp. 1-6.
- [3] S. J. Tong, A. Same, M.A. Kootstra, and J.W. Park, "Off-grid photovoltaic vehicle charge using second life lithium batteries: An experimental and numerical investigation," *Appl. Energy*, vol. 104, pp. 740–750, Apr. 2013.
- [4] B. Gohla-Neudecker, M. Bowler, and S. Mohr, "Battery 2nd life: Leveraging the sustainability potential of EVs and renewable energy grid integration," in *Proc. Int. Conf. Clean Elect. Power*, 2015, pp. 311–318.
- [5] S. U. Kim, P. Albertus, D. Cook, C. W. Monroe, and J. Christensen. "Thermoelectrochemical simulations of performance and abuse in 50-ah automotive cells," *J. Power Sources*, vol. 268, pp. 625-633, 2014.
- [6] Deliverable 9.8 -Report on Mobile Battery Test Platform and Results of the Measurements, Green eMotion Project Published Document. [Online]. Available: <https://www.greenemotion-project.eu/>

Author Index

C

Cheng K.W.E 6

D

D. H. Wang 11

J

Jinhao Ruan 1

J. Mei 11

K

K.W.E. Cheng 11

S

Shisong Wang 1

S. Raghu Raman 11

Y

Yuanxiong Duan 1

Y.C. Fong 11

Z

Zhanghai Shi 1

Submission Details

Only online submission will be accepted. Please first register and submit online. The paper is in double-column and is similar to most IET or IEEE journal formats. There is no page limit. Any number of pages of more than 6 will be subjected to an additional charge.

The paper guidelines can be downloaded using the link: <http://perc.polyu.edu.hk/apejournal/>

Any queries, please contact Prof. Eric Cheng, Publishing Director of APEJ, Dept. of Electrical Engineering, The Hong Kong Polytechnic University, Hung Hom, Hong Kong. Email: eeecheng@polyu.edu.hk Fax: +852-2330 1544

Any secretarial support and production related matters, please contact Dr. James Ho, Power Electronics Research Centre, The Hong Kong Polytechnic University, Hung Hom, Hong Kong. Email: eeapej@polyu.edu.hk Tel: +825-3400 3348 Fax: +852-3400 3343

Publication Details

The journal will be published 2-3 times a year. The first issue was published in 2007. Response time for paper acceptance is within 3 months.

Financial Charge

All the accepted papers will be printed without charge for 6 or less pages. An additional page charge is HK\$100 per page. A hardcopy of the journal will be posted to the corresponding author free of charge. Additional copies of the journal can be purchased at HK\$200 each. The charge includes postage and packing.

All Chinese Papers will be subjected to a translational fee of HK\$350 per page. It will be charged when the paper is accepted for publication.

Advertising

Advertisement is welcome. Full page advertisement is HK\$1000. For colour advertisements, the amount is doubled. All the advertisements will be both posted online in the journal website and hardcopy of the journal.

For advertising enquires and details, please contact Ms. Anna Chang, eeapej@polyu.edu.hk.

Tel: +852-3400 3348, Fax: +852-3400 3343

For payment, please send your cheque, payable to 'The Hong Kong Polytechnic University, address to Ms. Kit Chan, Secretary of APEJ, Dept. of Electrical Engineering, The Hong Kong Polytechnic University, Hung Hom, Hong Kong.'